Wind and Structures, *Vol. 29, No. 5 (2019) 339-359*
DOI: https://doi.org/10.12989/was.2019.29.5.339

Behaviour and design of guyed pre-stressed concrete poles under downbursts

Ahmed M. Ibrahim[1,2] and Ashraf A. El Damatty*[1,2]

[1]Department of Civil and Environmental Engineering. Western University, London, ON, Canada.
[2]Structural Engineering Department. Faculty of Engineering, Cairo University, Giza, Egypt

(Received April 26, 2018, Revised August 22, 2019, Accepted September 7, 2019)

Abstract. Pre-stressed concrete poles are among the supporting systems used to support transmission lines. It is essential to protect transmission line systems from harsh environmental attacks such as downburst wind events. Typically, these poles are designed to resist synoptic wind loading as current codes do not address high wind events in the form of downbursts. In the current study, the behavior of guyed pre-stressed concrete Transmission lines is studied under downburst loads. To the best of the authors' knowledge, this study is the first investigation to assess the behaviour of guyed pre-stressed concrete poles under downburst events. Due to the localized nature of those events, identifying the critical locations and parameters leading to peak forces on the poles is a challenging task. To overcome this challenge, an in-house built numerical model is developed incorporating the following: (1) a three-dimensional downburst wind field previously developed and validated using computational fluid dynamics simulations; (2) a computationally efficient analytical technique previously developed and validated to predict the non-linear behaviour of the conductors including the effects of the pretension force, sagging, insulator's stiffness and the non-uniform distribution of wind loads, and (3) a non-linear finite element model utilized to simulate the structural behaviour of the guyed pre-stressed concrete pole considering material nonlinearity. A parametric study is conducted by varying the downbursts locations relative to the guyed pole while considering three different span values. The results of this parametric study are utilized to identify critical downburst configurations leading to peak straining actions on the pole and the guys. This is followed by comparing the obtained critical load cases to new load cases proposed to ASCE-74 loading committee. A non-linear failure analysis is then conducted for the three considered guyed pre-stressed concrete transmission line systems to determine the downburst jet velocity at which the pole systems fail.

Keywords: guyed poles; transmission line structures; pre-stressed concrete poles; HIW-downbursts; finite element modelling

1. Introduction

Transmission lines are one of the most critical infrastructural elements all over the globe. Any deficiency in such structures can seriously affect people`s lives and activities. High intensity wind (HIW) events in the form of downbursts represent a major threat on transmission line structures. A downburst is defined as a violent downdraft of moist and cold air that suddenly impinges to the ground and spreads horizontally as described by Fujita (1985). Li (2000) stated that downbursts are the reason for more than 90% of weather-related failures. In China, 18 transmission towers carrying 500 kV lines and 60 towers carrying 110 kV lines collapsed due to strong wind events such as downbursts, tornadoes and typhoons (Zhang 2006). In Canada, many of transmission line structures failed in the past twenty years as a result of downbursts such as those reported by Manitoba Hydro (Mccarthy and Melsness 1996) and Hydro One, Ontario, in 2006. In 2016, 23 transmission towers failed during a series of downburst events in Australia (Australian Wind Alliance, 2016).

Many studies have been conducted to assess the response of transmission line structures under downburst loading. Shehata *et al*. (2005) developed and validated a finite element model to simulate the behavior of a guyed transmission line system under downbursts. Shehata and El Damatty (2007) conducted a parametric study by varying the downburst size and location to obtain the critical downburst configurations acting on guyed transmission line structures. Yang and Zhang (2016) conducted two cases studies involving the structural analysis of transmission towers under downbursts. Wang *et al.* (2009), Darwish *et al*. (2010), Darwish and el Damatty (2011) and Ladubec *et al*. (2012) also performed a number of studies on the effect of downburst forces on transmission lattice steel towers. Transmission line conductors' response under downbursts was investigated by Aboshosha and El Damatty (2014). Aboshosha and El Damatty (2014) developed a numerical technique to investigate the behavior of transmission line conductors under downburst loading taking into account the non-linear behavior of the conductors including sagging, pre-tensioning forces and insulator's stiffness.

El Damatty and Elawady (2018) summarized the major findings of the attempts made in the literature during the past decade to study the effect of downbursts on lattice steel transmission line structures. Despite the complexity of the downburst wind field and the fact that the downburst

*Corresponding author, Professor
E-mail: damatty@uwo.ca

Copyright © 2019 Techno-Press, Ltd.
http://www.techno-press.com/journals/was&subpage=7
ISSN: 1226-6116 (Print), 1598-6225 (Online)

location relative to the tower significantly affects the response, El Damatty and Elawady (2018) proposed three simplified critical downburst load cases to be considered in the design and analysis of lattice steel transmission line structures under downbursts. In each load case, the velocity profile along the towers' height and the conductors' spans are provided. Those simplified load cases provide an envelope for the maximum responses of a number of lattice steel transmission towers under a large number of possible downburst load configurations.

According to the supporting system, transmission line systems can be supported by lattice steel towers or pole-type structures. Few studies have assessed the behavior of pre-stressed concrete pole structures under downbursts. Ibrahim *et al*. (2017) developed and validated a non-linear finite element model to assess the behavior of a pre-stressed concrete pole under downbursts and tornadoes. A parametric study was conducted to obtain the downburst critical configurations which lead to the maximum straining actions on a self-supported pole. In addition to that, a non-linear failure analysis was performed to determine the critical downburst jet velocity at which the pole experienced collapse. The concrete and pre-stressing strands' non-linear properties such as cracking, tension stiffening, creep, shrinkage and relaxation were taken into account in the analysis.

In the current study, the finite element model developed and validated by Ibrahim *et al.* (2017) is utilized to study the performance of guyed pre-stressed concrete poles under downbursts. Three guyed pre-stressed concrete pole systems with different spans are designed to remain un-cracked under normal synoptic wind speed of 40 m/sec based on the provisions of ASCE 74 (2010) and ASCE 123 (2012). A parametric study is conducted on the three guyed transmission line pre-stressed concrete pole systems taking into account the variation of the size and location of the downburst event to identify the critical configurations which will lead to the maximum bending moments at the poles and the maximum tension forces in the guys. This is followed by a comparison made between the maximum responses obtained from the parametric study and the envelope of the critical downburst load cases proposed by El Damatty and Elawady (2018) for lattice transmission towers. The purpose of the comparison is to assess if the proposed downburst load cases can be applied to the guyed pre-stressed concrete pole structures. Finally, a non-linear failure analysis is conducted to determine the downburst jet velocity (V_j) at which the guyed pole systems are expected to fail.

2. Numerical model

The localized nature of the downburst wind events in addition to the non-linear behavior of the transmission line conductors and guyed pre-stressed concrete poles make the prediction of the response of the guyed pole systems a challenging task. As such, a sophisticated numerical model is developed to assess the behavior of guyed pre-stressed concrete pole structures under downbursts. conductors' reactions are predicted using the computationally efficient semi- analytical technique developed and validated by Aboshosha and El Damatty (2014). Thirdly, the non-linear finite element model developed and validated by Ibrahim *et al.* (2017) is utilized to obtain the straining actions in the poles and the guys.

2.1 Downburst forces

Wolfson *et al*. (1985), Fujita (1990), Gast and Schroeder (2003), Choi (2004) and Holmes *et al*. (2008) have made a few attempts to obtain the downburst field measurements. However, obtaining full scale data for such localized events is extremely hard. As such, numerical simulation of downbursts is considered a useful tool to estimate wind field velocities. A Computational Fluid Dynamics (CFD) model was developed by Hangan *et al*. (2003). The downburst outflow in this model consists of two velocity components: radial (horizontal) component (V_{RD}) and axial (vertical) component (V_{VL}). The factors affecting the values of the velocity components at a certain point are its location relative to the downburst center and its height above the ground. The wind field associated with the downburst is mainly affected by the parameters V_j, D_j, R and θ as shown in Fig. 1.

As shown in Fig. 1 the location of the center of the downburst with respect to the pole center is determined by the polar coordinates (distance (R) and the angle (θ)). The downburst intensity is defined by its jet diameter (D_j) and its jet velocity (V_j).

The downburst loads are obtained from the wind field. The velocity wind field is transformed into forces using the procedure provided in the ASCE-74 (2010) based on the following equation

$$F_{wi} = \frac{1}{2}\rho_a \, G C_f \, A (Z_v V_i)^2 \qquad (1)$$

Where F_{wi} is the force developing in the *i* direction, ρ_a is the density of air = 1.225 (Kg/m^3), G is the gust factor , C_f is the drag force coefficient, A is the nodal projected area perpendicular to *i* direction, Z_v is the terrain factor and V_i is the downburst velocity in the *i* direction (units m/sec). For conductors and circular concrete poles, the value of the drag coefficient is taken equal to 1.0 according to ASCE-74 (2010) guidelines, and the same value is recommended for gust and terrain.

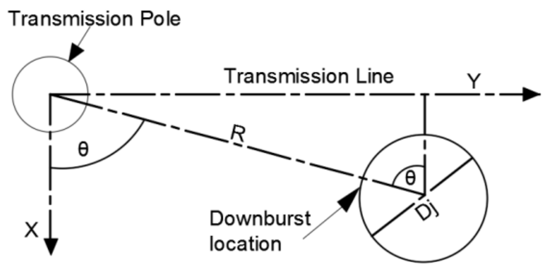

Fig. 1 Downburst Parameters

Table 1 Pre-stressed concrete pole properties

Unsupported Height (m)	Outer Top Diameter (mm)	Outer Bottom Diameter (mm)	Inner Top Diameter (mm)	Inner Bottom Diameter (mm)	Number of M10 low relaxationStr ands	Concrete compressive strength (N/mm^2)
25.5	281	459	143	321	20	75.8

Table 2 Conductors' properties

Projected area (m^2)	Weight per unit length (N/m)	Insulator Length (m)	Sag Value relative to the span	Cross arm length (m)
0.096	30	2.5	2%	2.4

Table 3 Guys' properties

Diameter (mm)	Guys Type	Pre-tensioning force (kN)	Guys grade based on (CSA-G12)	RBS based on ASCE-91(1997) (kN)
12	7-wire Strands	10	1300	120

2.2 Modeling of conductors

Conductors' reactions are predicted using the analytical technique developed by Aboshosha and El Damatty (2014). This technique accounts for the variation of the loads along the conductor spans, insulators flexibility and the non-linear behaviour of the conductors including sagging and pre-tensioning forces.

2.3 Modeling of guyed pre-stressed concrete poles

2.3.1 Modeling of the pre-stressed concrete poles

The non-linear finite element model developed and validated by Ibrahim *et al.* (2017) is utilized to simulate the pre-stressed concrete poles behaviour. Frame elements are used to model the pre-stressed concrete poles. The finite element model accounts for the non-linear behavior of pre-stressed concrete poles, the cracking and non-linear behavior of concrete, in addition to the long-term effects such as creep, shrinkage and relaxation.

2.3.2 Modeling of the guys

The guys are modelled using three non-linear dimensional frame elements with two nodes and six degrees of freedom per each node (three translational and three rotational). The stiffness of the guys depends on the applied pre-tensioning force. The guys can carry tension forces up to their rated breaking strength (RBS) as assigned by ASCE 91(1997). When the compression force in the guy exceeds the pre-tensioning force, the guy is assumed to slack.

The foundations design and analysis are not considered in the current study. However, the maximum straining actions at the pole base can be obtained from the study and can be used to design the foundations.

3. Considered Guyed concrete pole properties

The numerical model described earlier is employed to study the behaviour of three guyed pre-stressed concrete pole systems under downbursts. The following steps are conducted in this study:

1- Perform a parametric study by changing the downburst size and location in order to determine the critical downburst configurations leading tomaximum effect on the guyed poles under a specific downburst jet velocity.
2- Compare the straining actions that develop in the guys and the poles under the critical downbursts configurations to the corresponding values obtained from applying the three load cases proposed by El Damatty and Elawady (2018).
3- Conduct a non-linear analysis for the guyed poles using this critical downburst configuration that considers post cracking behaviour in order to determine the downburst jet velocity that would lead to a full collapse of the pole or the guys. The failure of a guy in tension occurs when the tension forces reaches its RBS.
4- While the failure in compression is due to slack ing. In compression, a guy slacks if it is subje cted to a compression force higher than the pr e-tensioning force.

Three transmission guyed pole systems with different conductor spans are considered in this study. The three systems are designed to remain un-cracked under a synoptic wind speed of 40 m/sec based on the ASCE 123 (2012) and ASCE 74 (2010) guidelines.

The three guyed pole systems have the following common geometric and material properties as shown in Tables 1-3.

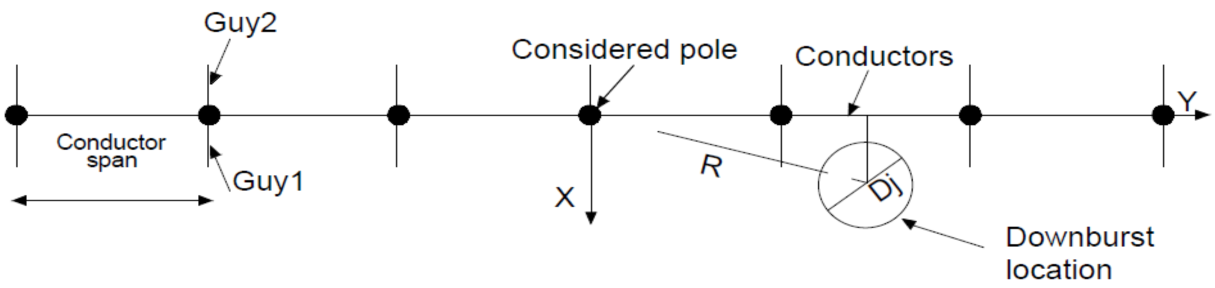

Fig. 2 Guyed pole systems (Plan View)

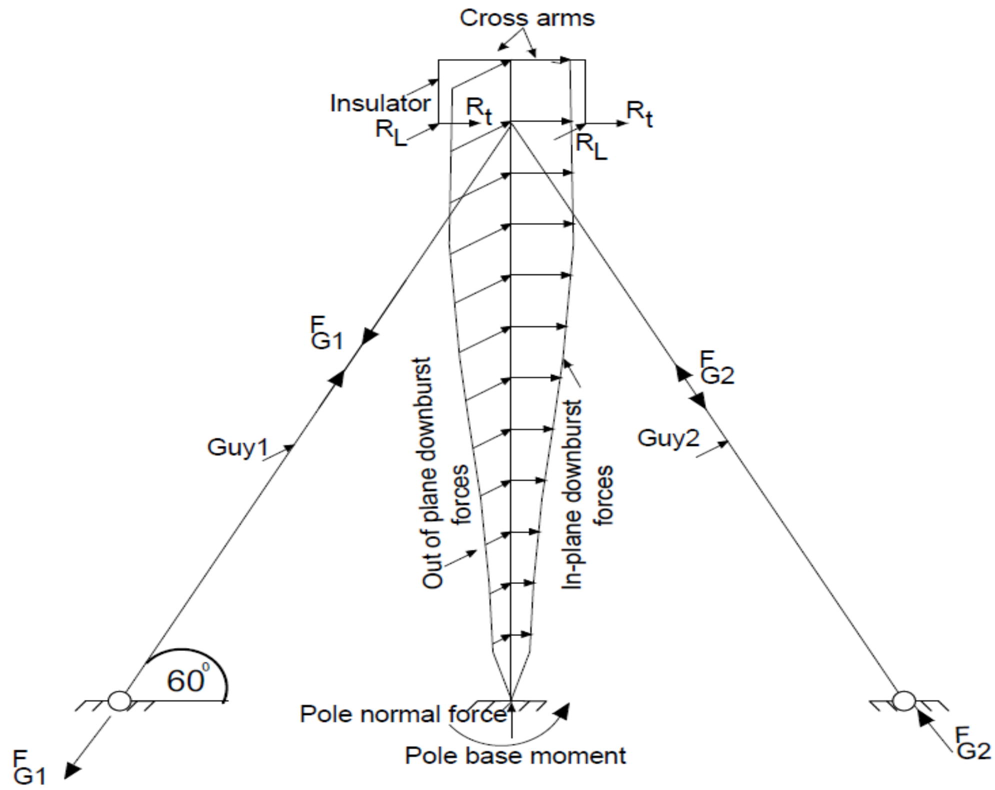

Fig. 3 Schematic diagram showing the guyed poles analysis under a downburst

For the guyed pole systems, two guys perpendicular to the conductors' line are used to support the pole. The guys' attachment points to the poles are at a height of 23 m similar to the conductors' attachment points to the insulators. The guys' angle of inclination with the ground is 60^0.

The three systems differ in terms of conductor spans which are assumed to be 100 m, 200 m and 300 m, respectively. Fig. 2 shows the layout of the guyed transmission pole systems.

3.1 Response of guyed poles under downbursts

Fig. 3 is introduced to help the reader in understanding the behaviour of the guyed pre-stressed concrete pole systems under in-plane and out of plane downburst loads. In this Figure, R_t is the transverse conductor reaction, R_L is the longitudinal conductor reaction, F_{G1} is the force developing in guy1 and F_{G2} is the force developing in guy2.

The downburst loads acting on a guyed pre-stressed concrete transmission pole system can be divided into two main parts: (1) loads acting on the conductors and (2) loads acting on the pole.

As mentioned above, the guys' orientation is normal to the direction of the transmission line conductors. In addition to that, the guys of the three pole systems are attached to the poles at the same height where the conductors are attached to the insulators. As such, the guys act as the support of the conductors and the transverse conductors' reactions are fully transferred to the guys.

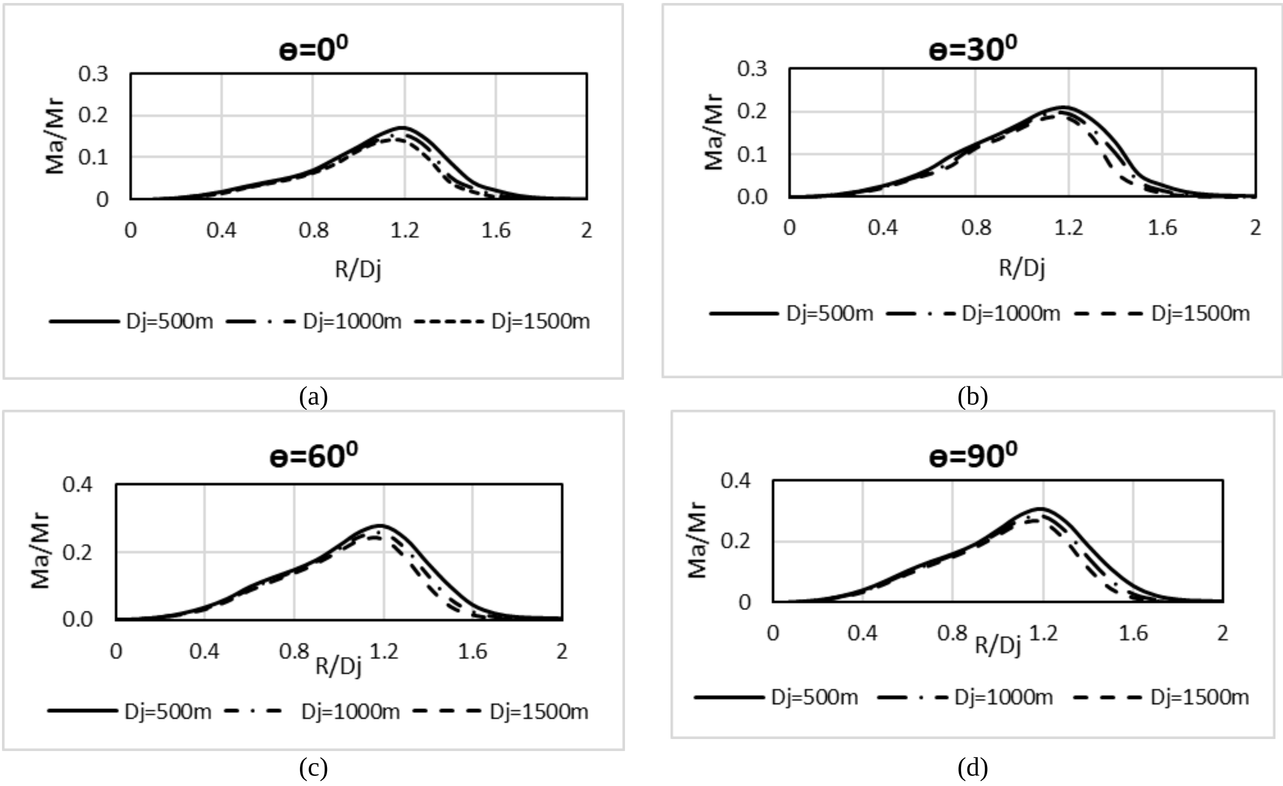

Fig. 4 (a)-(d) Variation of (M_a/M_r) with R/D_j

It should be noted that the guys only resist the component of the applied loads acting in a direction along its axes. Based on that, the conductors' longitudinal reactions are resisted only by the pole and the guys do not contribute in the resistance of those reactions.

The downburst loads acting on the pole are resolved into two components. The first component is in the direction perpendicular on the transmission lines (i.e., along with the guys' axes direction), while the second component is in the direction normal to the guys axes (i.e., along with the transmission lines direction). The first component is resisted by both the pole and the guys based on the relative stiffness between them. Meanwhile the second component is only resisted by the pole which acts as a cantilever pole in this case.

It should be noted that based on all the possible downburst configurations and the alignment of the guys with respect to the transmission lines of the three poles studied, guy1 is always subjected to tension forces while guy2 is usually subjected to compression forces. If the compression force guy2 due to both the in-plane forces acting on the poles and the conductors' transverse reactions exceeds the value of the pre-tensioning force (10 kN), guy2 will slack. In this case, only guy1 and the pole will support the guyed pole system while being subjected to the downburst. It is worth to mention that the value of the tension force that developed in guy1 in such cases exceeds 10 kN.

4. Downburst parametric study

The three guyed transmission poles designed to remain un-cracked under normal wind loads corresponding to reference wind speed of 40 m/sec are considered for the downburst analysis. In this section, a parametric study is conducted on three different guyed pre-stressed concrete pole systems. A total number of 924 downburst load configurations are applied to each of the three systems. The objective is to determine the configurations that lead to maximum bending moment, tension and compression forces on each of the three poles and the guys.

The parametric study is conducted for a fixed value for the jet velocity V_j= 40m/sec. The downburst configuration is defined by the jet diameter D_j and the geometric parameters (R and θ) as shown in Fig. 1. In the parametric study, the downburst jet diameter is assumed to be varying from 500 m to 1500 m with an increment of 100 m. The ratio R/D_j is varied from 0 to 2 with an increment of 0.1, while the angle (θ) is varied between 0^0 and 90^0 with an increment of 30^0. The overturning moment (M_a) normalized by the pole ultimate capacity (M_r) at the pole base is determined for each configuration. The tension and compression forces in the guys are identified as well. In addition to that, the downburst velocities distributions across the conductors' spans and the poles' height are presented for the critical load cases.

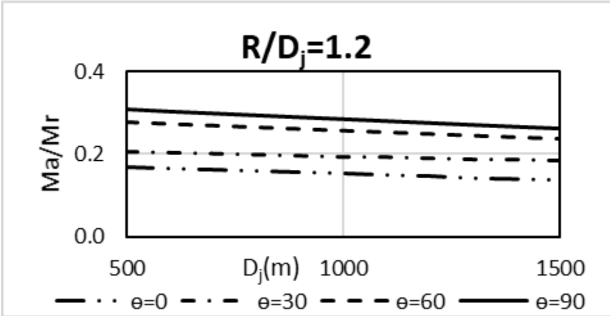

Fig. 5 Variation of (M_a/M_r) with D_j

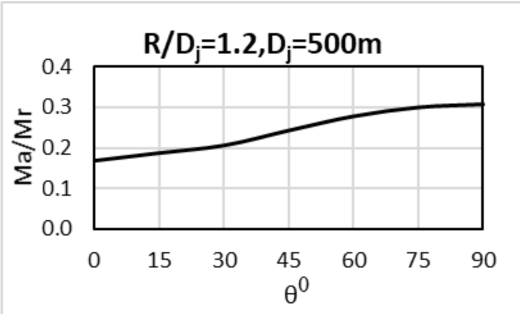

Fig. 6 Variation of (M_a/M_r) with θ

4.1 Results of the Guyed pole system with conductor span 100 m

4.1.1 Base moment

The results of the parametric study are presented in Figs. 4(a)-4(d). Each figure corresponds to a specific value of "θ" and shows the variation of the ratio (M_a/M_r) with D_j and (R/D_j).

The figures indicate that the maximum (M_a/M_r) ratio occurs consistently at R/D_j=1.2. As such, the processing of the results is then focused on this ratio.

Fig. 5 shows the variation of (M_a/M_r) with D_j and θ for R/D_j =1.2, while Fig. 6 shows the variation of the same ratio with θ for R/D_j =1.2 and D_j=500 m.

The figures indicate that the absolute maximum value for the ratio (M_a/M_r) occurs at the configuration D_j=500 m, R/D_j =1.2 and θ =90^0, which can be considered the critical downburst configuration. This configuration leads to maximizing the bending moments acting on the pole base.

At θ=0^0, the conductors' reactions are only transversal. As such, the conductors' reactions are totally transferred to the guys. The downburst load on the pole is shared between the pole and the guys. It is worth to mention that the contribution of the guys in resisting the downburst load on the pole in this case is the highest among all the other downburst configurations. This is attributed to the fact that at θ=0^0 the entire downburst load component is in the direction of the guys and no downburst loads are acting on the pole in the out-of-plane.

By increasing θ, the transverse conductors' reactions decrease. As a result, the guys carry less load. Longitudinal conductors' reactions as well as the downburst load component which acts normal to the guys' axes are resisted by the poles. As mentioned before, the guys are not able to resist the loads perpendicular to its plane and the pole acts as a cantilever in resisting the out of plane loads.

At θ=90^0, the conductors are unloaded. In this case the pole acts as a cantilever while resisting the out-of-plane downburst wind loads acting on it without any support from the guys. This explains why the configuration of θ=90^0 is considered as the most critical configuration which lead to maximum bending moments on the guyed pole systems.

4.1.2 Forces in guy1 (FG_1)

The effect of changing downburst configurations on the forces developing in guy1 are presented in Fig. 7(a)-7(d). Each figure corresponds to a specific value of "θ" and shows the variation of the guy1 tension forces (F_{G1}) with D_j and (R/D_j).

As shown in the figures, the forces in guy1 are tension for all the downburst possible configurations. The critical case at which the tension of guy1 reaches its maximum value occurs when R/D_j=1.2. As mentioned before, the guys are not contributing in resisting the downburst load when θ=90^0.

The magnitude of the forces in both guys are the same unless guy2 is subjected to a compression force greater than the guys' pre-tensioning force, which is 10 kN. Once the compression force in guy2 exceeds 10 kN, guy2 slacks and the whole transverse conductor reaction is transferred to guy1. In such cases, the tension force in guy1 exceeds 10 kN. The following figures show the variation of guy1 forces with D_j and θ.

The variation of D_j does not significantly affect the value of the tension forces that develop in guy1. By studying the variation of the tension forces values in

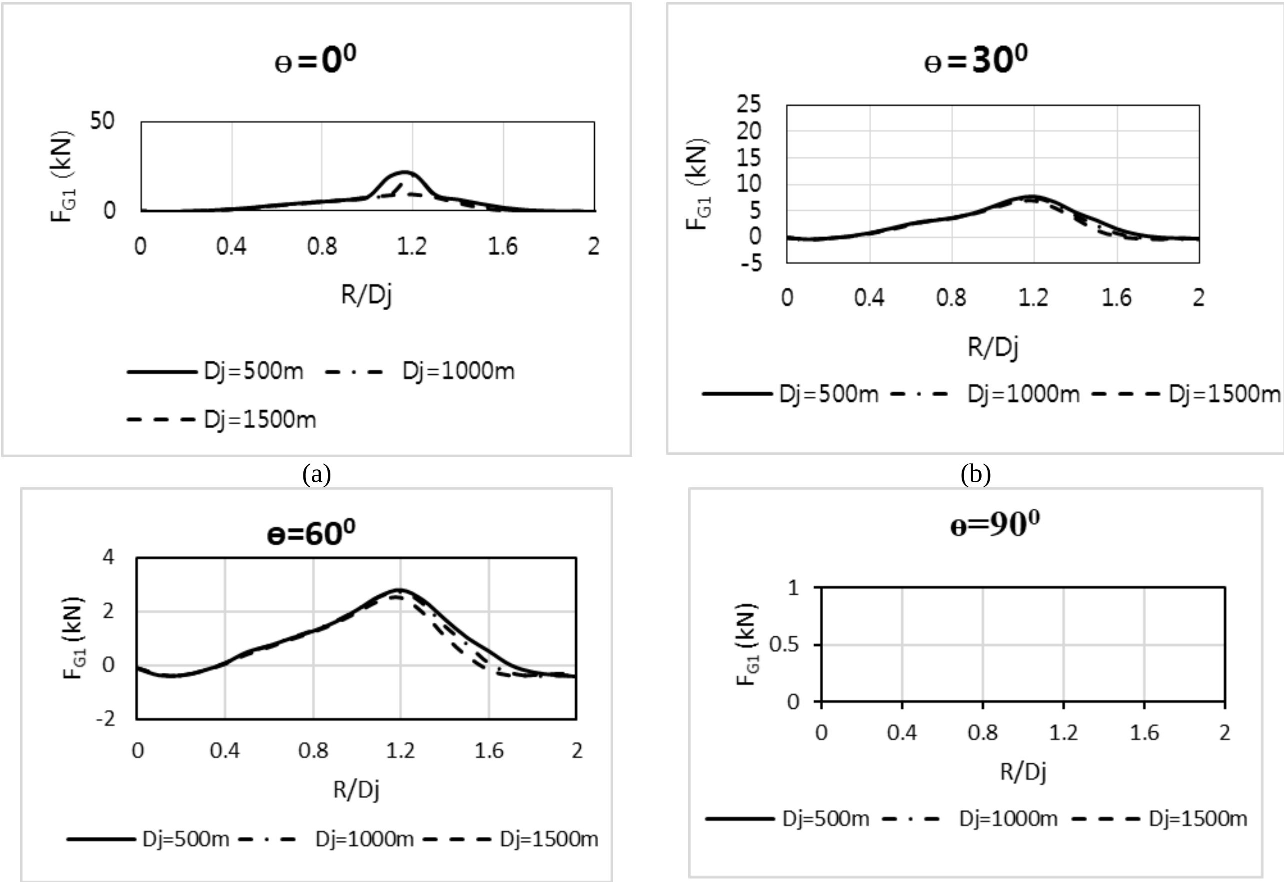

(c) (d)

Fig. 7 (a)-(d) Variation of F_{G1} with R/D_j

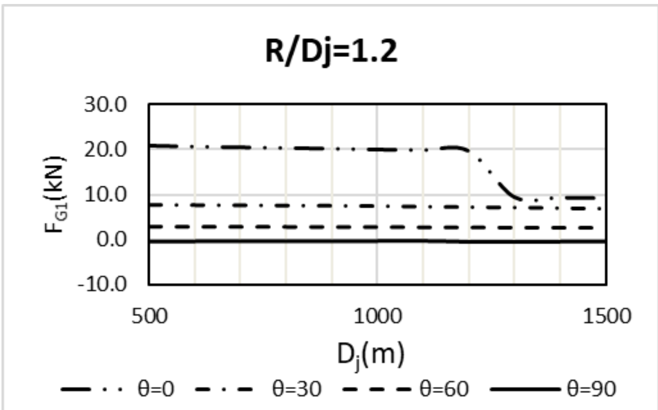

Fig. 8 Variation of F_{G1} with D_j

guy1with θ, it is found that $\theta=0^0$ is the most critical configuration which leads to the maximum tension value for FG1. For $\theta=0^0$, D_j between 500 m and1200 m and $R/D_j=1.2$, FG_1 exceeds 10 kN which means that guy2 slacked in these downburst configurations. This finding is shown later in Figs. 10 and 11.

This finding is shown later in Figs. 10 and 11.

It can be noted from Fig. 9 that with the increase of θ, the force in guy1 decreases until its contribution becomes zero at $\theta=90^0$. The higher values of the tension forces occurring in some cases at $\theta=0^0$ and $\theta=15^0$ are attributed to the slacking of guy2 in those cases. The critical downburst configuration which leads to the highest tension forces acting on guy1 occurs when $\theta=0^0$, $R/D_j=1.2$ and $D_j=500$ m.

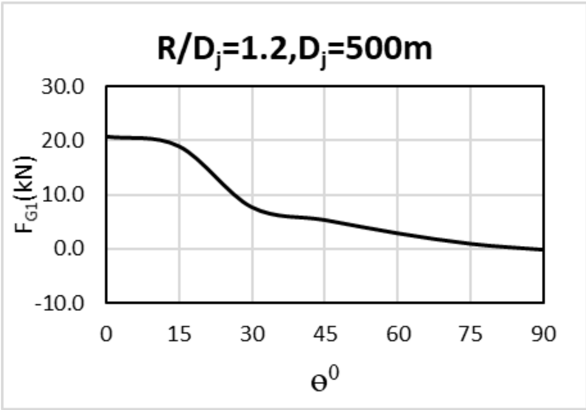

Fig. 9 Variation of F_{G1} with θ

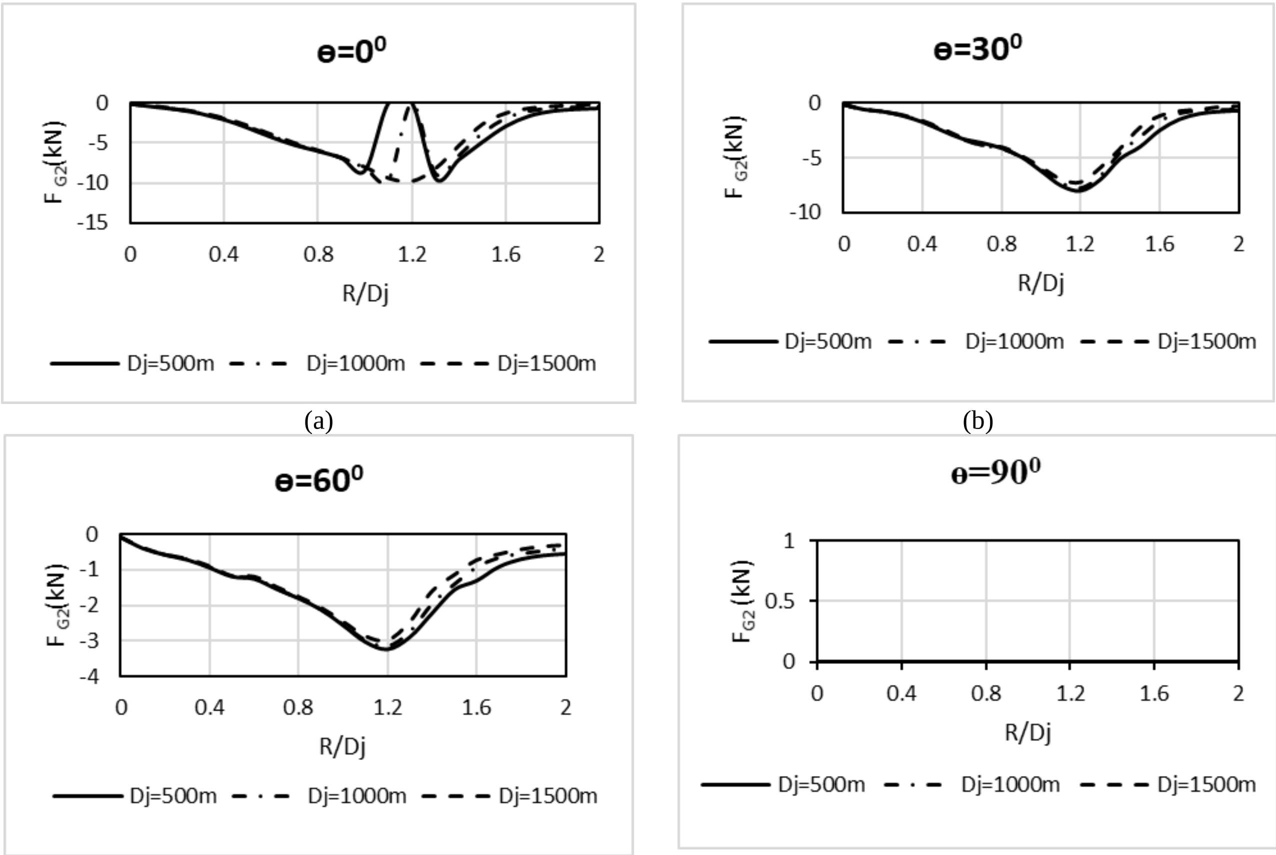

(a) (b)

(c) (d)

Fig. 10 (a)-(d) Variation of F_{G2} with R/D_j

4.1.3 Forces in guy2

The following figure shows the variation of the guy 2 compression forces (F_{G2}) with R/D_j and D_j for each downburst case.

The figure indicates that the compression force that develops in guy2 increases when the ratio (R/D_j) approaches 1.2. However, when the compression force in the guy exceeds the pretension force (10kN), the guy slacks and loses its stiffness. This case is shown in Fig. 10(a). The following figures show the variation of guy2 forces with D_j and θ.

As shown in the figures, slacking occurs when the compression force in guy2 exceeds the pretension force (10kN). This occurs in the cases where θ=0^0 and D_j is ranging between 500 and 1200 m. It should be mentio ned that at θ=90^0, the forces in guy2 are equal to zero.

As such, the critical downburst load case which results in maximum tension force in guy1 and slacking of guy 2 is corresponding to θ=0^0, D_j=500m and R/D_j=1.2. At this critical load case, the distribution of the transverse forces on the conductors leads to the maximum conductor resultant horizontal reaction which is totally resisted by the guys.

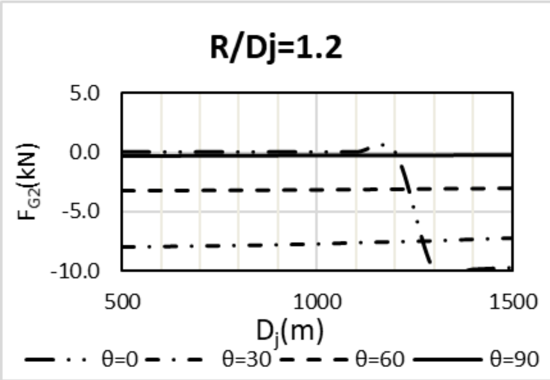

Fig. 11 Variation of F_{G2} with D_j

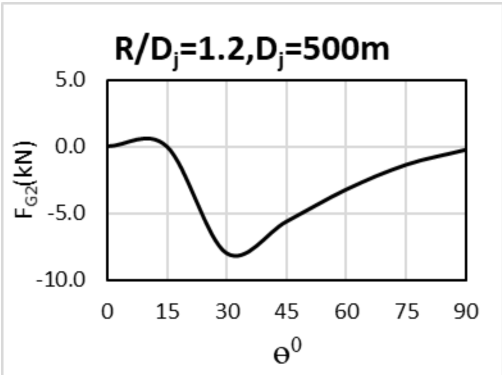

Fig. 12 Variation of F_{G2} with θ

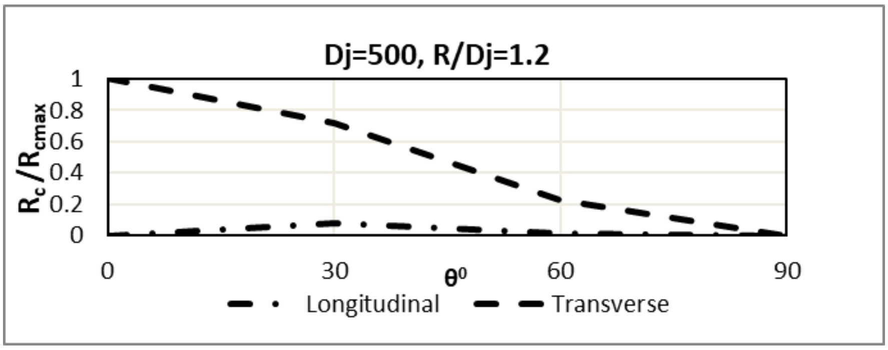

Fig. 13 Variation of conductor reactions with θ

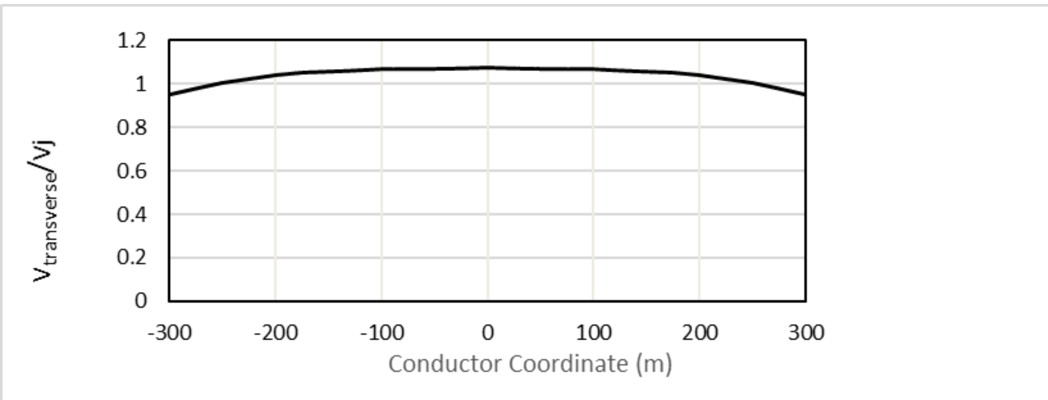

Fig. 14 Variation of $V_{transverse}$ along the conductor span

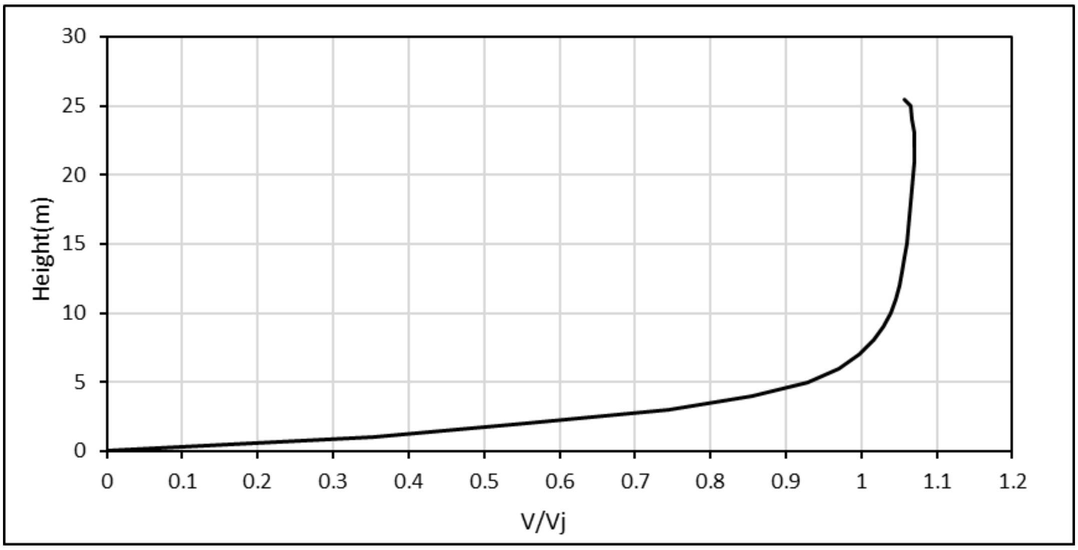

Fig. 15 Downburst velocity distribution along the pole height

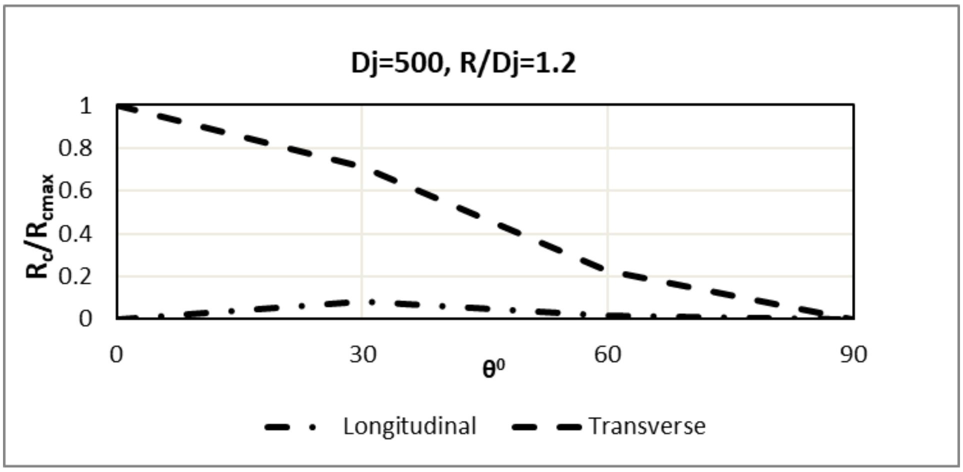

Fig. 16 Variation of conductor reactions with θ

The variation of the conductors longitudinal and transverse reactions (R_c) normalized by the maximum resultant horizontal conductor reaction (R_{cmax}) with θ at D_j=500 m and R/D_j=1.2 is shown in Fig. 13.

The figure indicates that the highest transverse reactions occurs when $\theta=0^0$. It should be noted that the values of the longitudinal reactions are relatively low if compared with the transverse ones. At the case of $\theta=0^0$, D_j=500 m and R/D_j=1.2, the downburst wind field is fully loading the two spans adjacent to the guyed pole under consideration with an average velocity of 1.07V_j. This is attributed to the fact that the jet diameter is greater than the sum of the two conductor spans (200 m) adjacent to the considered guyed pole. Fig. 14 shows the distribution of the transverse downburst wind velocities ($V_{transverse}$) at the critical load case along the six conductor spans.

The distribution of the radial velocity along the pole height at the critical load case is shown in Fig. 15. The plots indicate that the downburst velocities along the pole height can reach up to 1.06 V_j.

4.2 Results of the Guyed pole system with conductor span 200 m

The figures showing the variation of the concrete p ole base moments and guys' forces with the D_j, R/D_j a nd θ for conductor span of 200 m are provided in App endix A. The critical case which gives the highest bas e moment on the pole is found to happen at R/D_j=1.2, $\theta=90^0$ and D_j=500 m, while the case which causes maximum tension forces on guy1 corresponds to R/D_j=1.2, $\theta=0^0$ and D_j=500 m. The variation of the conductors longitudinal and transverse reactions (R_c) normalized by the maximum resultant horizontal conductor reaction (R_{cmax}) with θ at D_j=500 m and R/D_j=1.2 is shown in Fig. 16.

In the case of $\theta=0^0$, D_j=500 m and R/D_j=1.2, the downburst wind field is fully loading the two spans adjacent to the guyed pole under consideration with velocity that reaches up to 1.06 V_j. That is attributed to the fact that the jet diameter is greater than the sum of the two conductor spans (400 m) adjacent to the considered guyed pole.

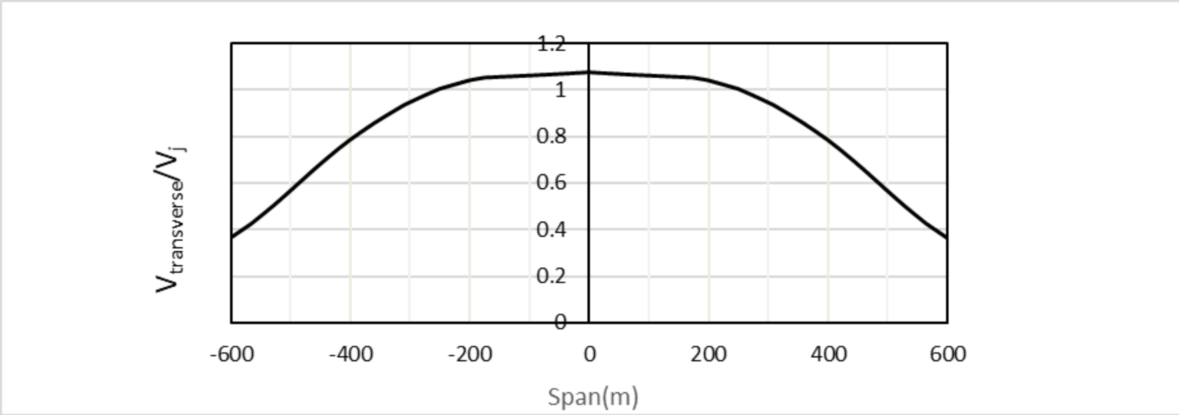

Fig. 17 Variation of $V_{transverse}$ along the conductor span

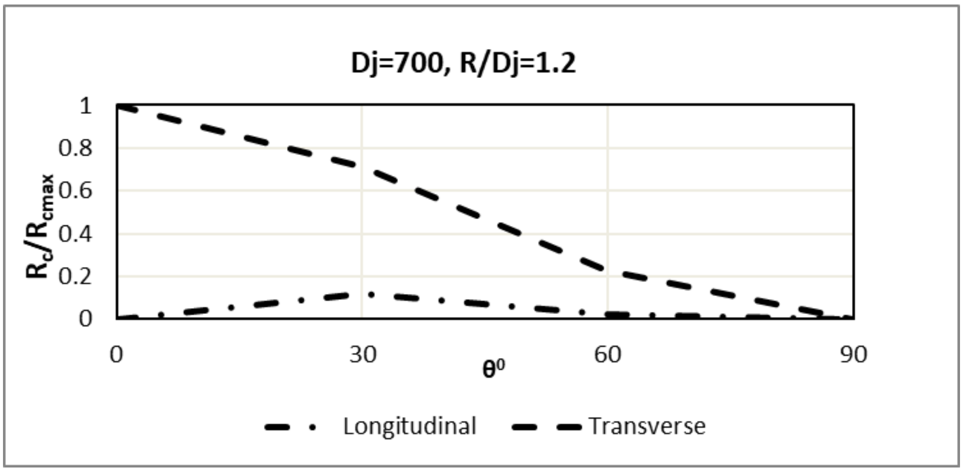

Fig. 18 Variation of conductor reactions with θ

Fig. 17 shows the distribution of the transverse downburst wind velocities ($V_{transverse}$) at the critical load case along the six conductor spans.

4.3 Results of the Guyed pole system with conductor span 300 m

The figures illustrating the variation of the concrete pole base moments and guys' forces with the change of D_j, R/D_j and θ for conductor span of 300 m are provided in Appendix B.

The critical case which gives the maximum base moment on the pole of a 300 m conductor span is found to be the same as for the 100 m and 200 m spans. (i.e., R/D_j=1.2, θ =90^0 and D_j=500 m). As such, it can be concluded that the maximum pole base moments are independent of conductor spans.

For the guys of the 300 m pole system, the case which causes maximum tension forces on guy1 is when R/D_j=1.2, θ =0^0 and D_j=700 m. The variation of the conductors' longitudinal and transverse reactions (R_c) normalized by the maximum resultant horizontal conductor reaction (R_{cmax}) with θ at D_j=700 m and R/D_j=1.2 is shown in the following figure.

To explain why the case D_j=700 m is more critical that the D_j=500 m case for the 300 m span, the transverse velocity distribution of the downburst load case of D_j=700 m is plotted along the span of the conductors and compared to the cases D_j=500 m, 600 m, 700 m, 800 m and 900 m, respectively.

It is obvious from the plots that for the case D_j=700 m, the velocities' magnitudes along the conductor spans is higher than the other cases. This leads to higher conductor reactions and consequently greater guys' forces.

The maximum compression force that develops in the poles due to the critical downburst wind loading cases is found to be in the order of 93 kN. The method described by Gere and Carter (1962) is utilized to obtain the buckling capacity of the tapered guyed transmission poles. It is found that the buckling capacity of the three considered pole systems is 145 KN. As such, bucking will not be critical issue for the guyed pre-stressed concrete poles under downburst loadings.

5. Comparison between the parametric study results and proposed critical load cases

El Damatty and Elawady (2018) proposed three critical load cases to simulate the effect of downbursts on

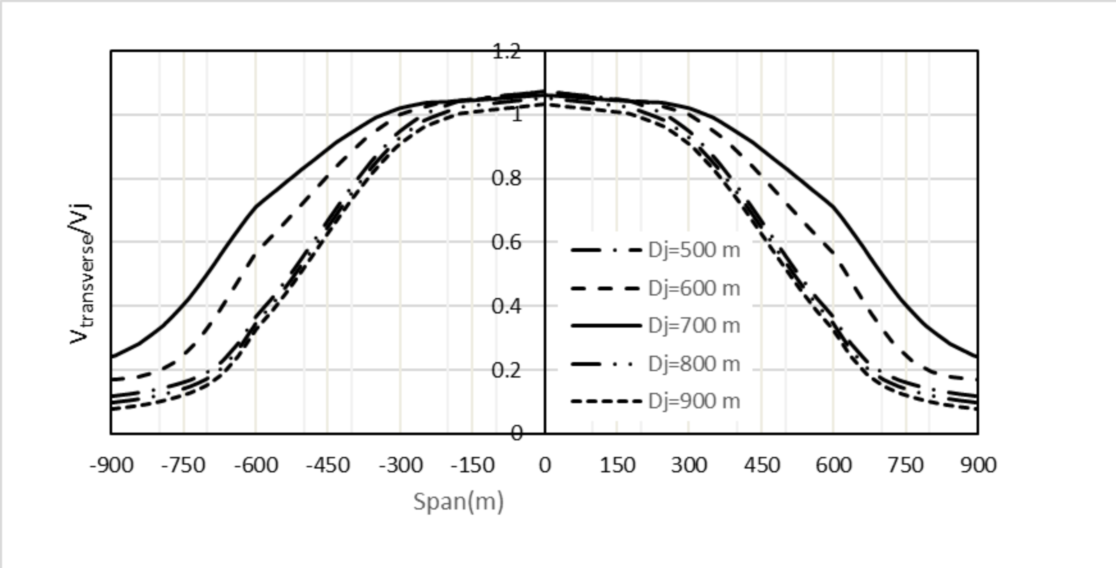

Fig. 19 Variation of $V_{transverse}$ along the conductor span

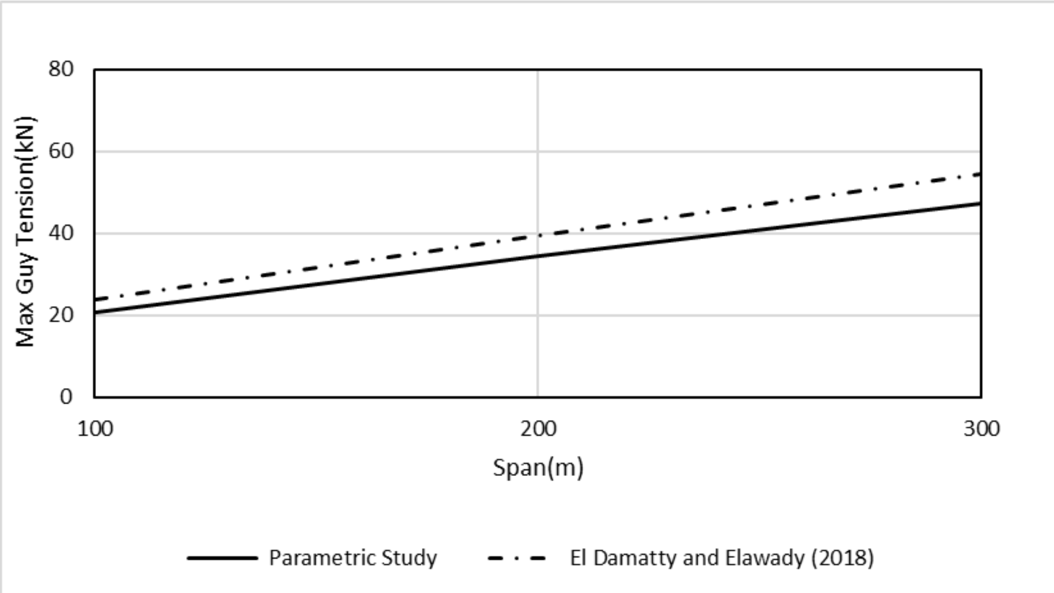

Fig. 20 Maximum Guy tension using parametric study and El Damatty and Elawady (2018) load cases

transmission line structures. In this section, the three load cases are applied on the three different guyed pre-stressed concrete pole systems. The maximum bending moment ratios (M_a/M_r) and maximum tension forces F_{G1} under the proposed load cases are obtained.

Those values are then compared to the corresponding values obtained from the parametric study conducted earlier in this study. The purpose is to check if the proposed load cases by El Damatty and Elawady (2018) can be applied for guyed pre-stressed pole structures under downbursts.

The three load cases proposed by El Damatty and Elawady (2018) are as follows:

Load case 1: ($\theta=0^0$)

In this load case, the pole is loaded with a vertical wind velocity profile of a value of 1.1 V_j in a direction normal to the transmission line, while the two conductors adjacent to the pole of interest are loaded with 0.92 V_j.

Load case 2: ($\theta=90^0$)

In this load case, the pole is loaded with a vertical wind velocity profile of a value of 1.1 V_j in a direction along with the transmission line. The conductors in this load case are unloaded.

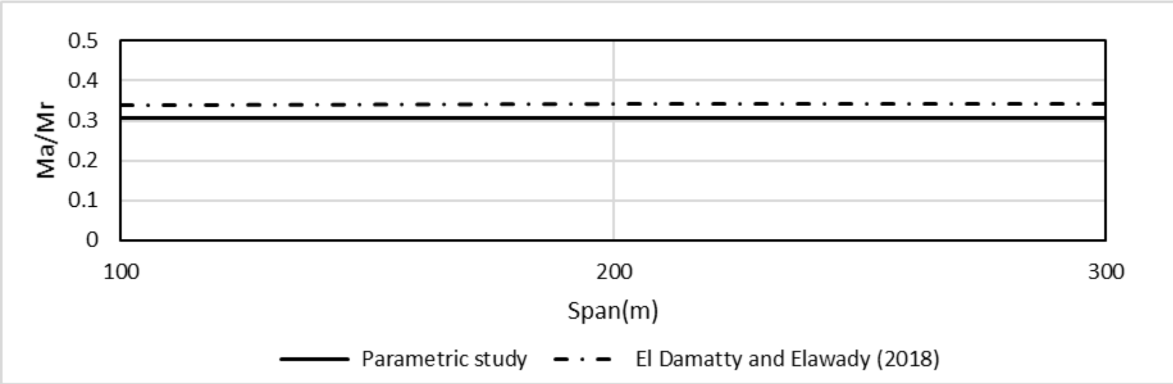

Fig. 21 Maximum pole base moment using parametric study and El Damatty and Elawady (2018) load cases

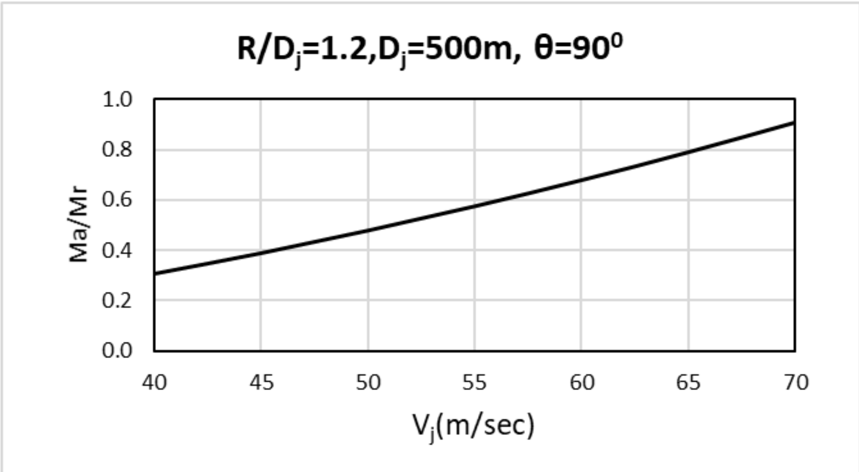

Fig. 22 Variation of maximum pole moment with V_j for different conductor spans

<u>Load case 3: (θ=30^0)</u>

This load case corresponds to a configuration where the line connecting the centers of the downburst and the tower forms an oblique angle with the conductors.

This configuration will result in a loading that has components parallel and perpendicular to the line. The vertical profiles of those two load components are provided by El Damatty and Elawady (2018) and they have maximum values of 0.75Vj and 0.43Vj, respectively. In this load case, the conductors are loaded with an unequal and a non-uniform velocity distribution on the spans adjacent to the tower of interest. This unequal loading is used to obtain the transverse conductor reaction. It should be noted that this load case lead to a longitudinal conductor reaction. The estimation of the conductor reactions under this load case is provided in Elawady and El Damatty (2016).
El Damatty and Elawady (2018) load cases are applied on the three pole systems and the maximum (M_a/M_r) and F_{G1} values are obtained and compared to the parametric study results in Figs. 20 and 21.

The comparison between the parametric study results and the proposed critical load cases shows a very good agreement. The difference between the maximum bending moments obtained from the current study and the corresponding ones proposed by El Damatty and Elawady (2018) is 3%, while the difference in the peak forces that develops in the guys is ranging between 4 to 6% based on the conductor span. El Damatty and Elawady (2018) load cases are found to be more conservative in the estimation of the maximum straining actions on the guyed pole systems. Based on that, the proposed load cases recommended by El Damatty and Elawady (2018) can be considered while simulating the guyed pre-stressed concrete pole systems under downbursts. Instead of performing 924 downburst cases, the peak responses of the guyed pre-stressed concrete transmission poles under downbursts can be evaluated by applying the simple load cases proposed by El Damatty and Elawady (2018). This will result in a significant saving in the computational time.

6. Failure analysis

After determining the critical downbursts configuration, a failure analysis is performed on the considered transmission pre-stressed pole to identify the downburst jet velocity at which the pole and the guys collapses. Regarding the poles failure analysis, it was mentioned

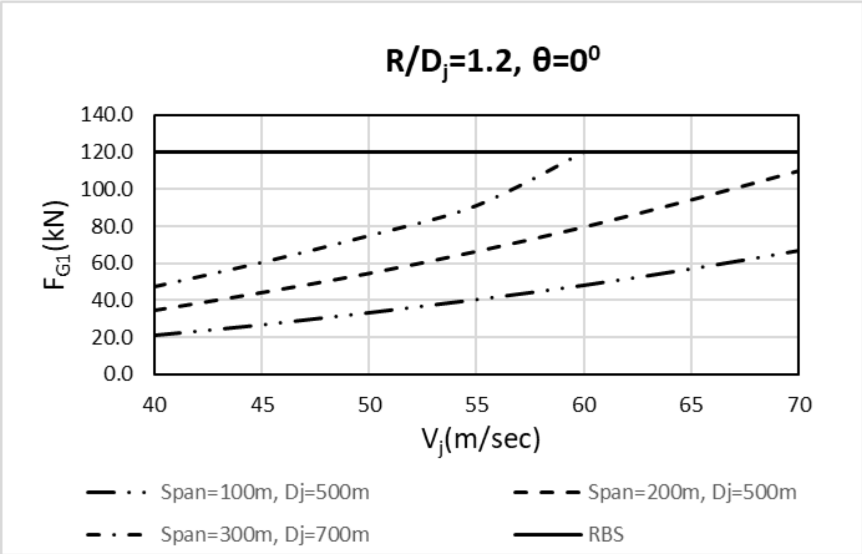

Fig. 23 Variation of maximum guy1 force with V_j for different conductor spans

earlier that the critical downburst configuration that affects the maximum bending moments developing in the guyed pole systems is independent of the spans. As such, only the 100 m pole system is considered in the failure analysis. The ratio (M_a/M_r) under downburst jet velocities varying between 40 and 70 (m/sec) with an increment of 5 (m/sec) is calculated and plotted in Fig. 22.

It can be noted from the figure that the maximum base moment at the pole does not reach to the ultimate pole capacity. This indicates that the guyed pre-stressed concrete poles, which are designed to remain un-cracked under normal wind speed of 40 m/sec, will not fail under a downburst jet velocity of 70 m/sec.

It is worth to mention that the concrete pole critical cross section is at the base. As such, the cracks occur at the base first. Once the cracks occur, the stiffness matrix of the pre-stressed concrete pole is updated. A new modulus of elasticity is calculated based on the applied moment and the cross-section's properties. More details can be found at Ibrahim *et al*. (2017).

The variation of the maximum guy tension of the pole with different jet velocities is then plotted for each span in Fig. 23. The configuration (R/D_j=1.2, $\theta=0^0$) is used to obtain the maximum guys' forces. Based on the results of the previous parametric study, the critical values of D_j for the 100, 200 and 300 m spans are considered to be 500 m, 500 m and 700 m, respectively.

It is found that guy1 reaches the rated breaking strength (120 kN) when the downburst jet velocity V_j exceeds 60 (m/sec) for the 300 m span. However, for spans 100 m and 200 m, guy1 does not reach the rated breaking strength.

7. Conclusions

In the current study, a numerical technique is utilized combining the following: 1) CFD model to simulate downbursts wind fields, 2) a semi-closed form solution that is capable of determining the conductor reactions under such localized high intensity wind events, and 3) a non-linear finite element model for guyed pre-stressed concrete pole structures that can predict the internal forces of such types of poles under downbursts. The main conclusions drawn from this study can be summarized in the following points:

1- The critical downburst configuration which leads to the maximum pole base moment is $\theta=90^0$, D_j=500 m and R/D_j=1.2.
2- The critical downburst configuration which leads to the maximum pole base moment is independent of the conductor spans.
3- The critical downburst configuration which leads to the maximum guys forces occurs at $\theta=0^0$, D_j=500m and R/D_j=1.2 for spans ranging from 100 to 200 m and when $\theta=0^0$, D_j=700 m and R/D_j=1.2 for a span of 300m.
4- The guyed pre-stressed concrete pole systems designed to remain un-cracked under normal wind speed of 40 m/sec do not collapse when their spans are ranging between 100 m and 200 m. However, the guys reach the rated breaking strength in the guyed concrete pole system that carries 300 m conductor spans when the jet speed exceeds 60 m/sec.
5- The previously developed load cases are found to be conservative and can be used in the design and analysis of guyed pre-stressed concrete pole transmission lines under downbursts.

Acknowledgments

The authors would like to acknowledge HYDRO ONE Company, Ontario, Canada and Natural Sciences and Engineering Council of Canada (NSERC) for funding this research.

References

Aboshosha, H. and El Damatty, A.A. (2014), "Effective technique for the reactions of transmission line conductors under high intensity winds", *Wind Struct.*, **18**(3), 235-252. http://dx.doi.org/10.12989/was.2014.18.3.235.

American Society of Civil Engineers (ASCE), (2010) "Guidelines for electrical transmission line structural loading", ASCE manuals and reports on engineering practice, No. 74, New York, NY, USA.

American Society of Civil Engineers (ASCE), (1997) "Design of guyed electrical transmission structures", ASCE Manuals and Reports on Engineering Practice, vol. 91, New York, NY, USA.

American Society of Civil Engineers (ASCE), (2012) "Prestressed Concrete Transmission Pole Structures", ASCE manuals and reports on engineering practice, No. 123, Reston, VA, USA.

Australian Standard/New Zealand Standard (AS/NZS) 7000, (2010) "Overhead line design detailed procedures", Standards Australia Limited/Standards New Zealand, North Sydney, Australia.

Australian Wind Alliance, (2016): http://www.windalliance.org.au/

Choi, E.C.C. (2004), "Field measurement and experimental study of wind speed profile during thunderstorms", *J. Wind Eng. Ind. Aerod.*, **92**(3-4), 275-290. https://doi.org/10.1016/j.jweia.2003.12.001.

Darwish, M., El Damatty A.A. and Hangan, H. (2010), "Dynamic characteristics of transmission line conductors and behaviour under turbulent downburst loading", *Wind Struct.*, **13**(4), 327-346. http://dx.doi.org/10.12989/was.2010.13.4.327.

Darwish, M. and El Damatty, A.A. (2011), "Behavior of self-supported transmission line towers under stationary downburst loading", *Wind Struct.*, **14**(5), 481-4.

Elawady, A. and El Damatty A.A. (2016), "Longitudinal force on transmission towers due to nonsymmetric downburst conductor loads", *Eng. Struct.*, **127**, 206-226. https://doi.org/10.1016/j.engstruct.2016.08.030.

El Damatty, A.A. and Elawady, A. (2018), "Critical load cases for lattice transmission line structures subjected to downbursts: Economic implications for design of transmission lines", *Eng. Struct.*, **159**, 213-226. https://doi.org/10.1016/j.engstruct.2017.12.043.

Fujita, T. (1985), "The downburst: microburst and macroburst", SMRP Research Paper 210, University of Chicago, USA.

Fujita, T. (1990), "Downbursts: meteorological features and wind field characteristics", *J. Wind Eng. Ind. Aerod.*, **36**, 75-86. https://doi.org/10.1016/0167-6105(90)90294-M.

Gast, K.D. and Schroeder, J.L. (2003), "Supercell rear-flank downdraft as sampled in the 2002 thunderstorm outflow experiment", *Proceedings of the 11th International Conference on Wind Engineering. ICWEIA*, 2233-2240.

Gere, J.M. and Carter, W.O. (1962), "Critical buckling loads for tapered columns", *J. Struct. Div- ASCE*, **88**(1), 1-12.

Hangan, H., Roberts, D., Xu, Z. and Kim, J. (2003), "Downburst simulation. Experimental and numerical challenges", *Proceedings of the 11th International Conference on Wind Engineering*, Lubbock, TX, USA.

Holmes, J., Hangan, H., Schroeder, J., Letchford, C. and Orwig, K. (2008), "A forensic study of the Lubbock-Reese downdraft of 2002", *Wind Struct.*, **11**(2), 137-152. http://dx.doi.org/10.12989/was.2008.11.2.137.

Ibrahim, A.M. and El Damatty, A.A., (2014), "Behaviour of Prestressed Concrete Poles under Downburst Loading", *Proceeding of ASCE conference*, Hamilton, ON, Canada.

Ibrahim, A.M., El Damatty, A.A. and Elansary A.M. (2017), "Finite element modelling of pre-stressed concrete poles under downbursts and tornadoes", *Eng. Struct.*, **153**, 370-382. https://doi.org/10.1016/j.engstruct.2017.10.047.

Ladubec, C., El Damatty, A.A. and El Ansary, A. (2012), "Effect of geometric nonlinear behaviour of a guyed transmission tower under downburst loading", *Proceedings of the International Conference on Vibration, Structural Engineering and Measurement*, Shanghai, China, Trans. Tech. Publications, 1240-1249.

Li, C.Q. (2000), "A stochastic model of severe thunderstorms for transmission line design", *Probablist. Eng. Mech.*, **15**(4), 359-364. https://doi.org/10.1016/S0266-8920(99)00037-5.

McCarthy, P. and Melsness, M. (1996), "Severe weather elements associated with September 5, 1996 hydro tower failures near Grosse".

Shehata, A., El Damatty, A.A. and Savory, E. (2005), "Finite element modeling of transmission line under downburst wind loading", *Finite Elem. Anal. Des.*, **42**(1), 71-89. https://doi.org/10.1016/j.finel.2005.05.005.

Shehata, A. and El Damatty, A.A. (2007), "Behaviour of guyed transmission line structures under downburst wind loading", *Wind Struct.*, **10**(3), 249-268 http://dx.doi.org/10.12989/was.2007.10.3.249.

Wang, X., Lou, W., Li, H. and Chen, Y. (2009), "Wind-induced dynamic response of high-rise transmission tower under downburst wind load", *J. Zhejiang Univ.*, **43**(8), 1520-1525.

Wolfson, M., DiStefano, J. and Fujita, T. (1985), "Low-altitude wind shear characteristics in the Memphis, TN area", *Proceedings of the 14th conference on severe local storms, American Meteorological Society*, Indianapolis, IN, USA., 322–7.

Yang, F. and Zhang, H. (2016), "Two case studies on structural analysis of transmission towers under downburst", *Wind Struct.*, **22**(6), 685-701. http://dx.doi.org/10.12989/was.2016.22.6.685.

Zhang, Y., (2006), "Status quo of wind hazard prevention for transmission lines and countermeasures", *East China Electric Power*, 34(3), 28-31.

CC

Appendix A

Results of the guyed pole with conductor spans of 200 m

9.1 Pole bending moment

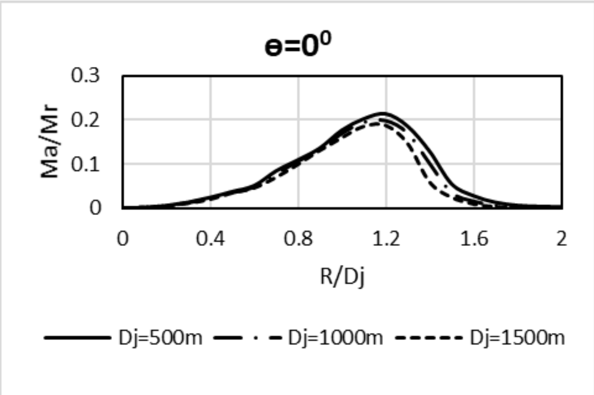

(a)

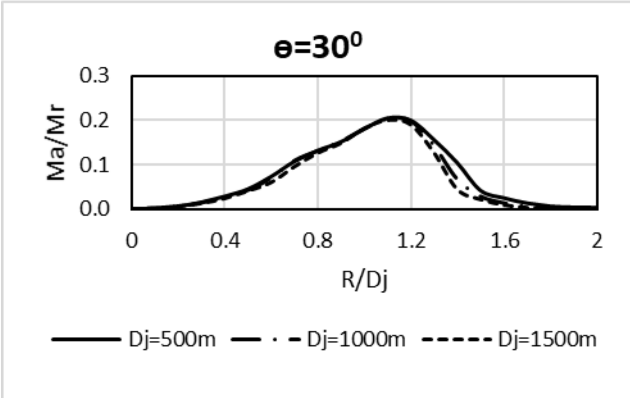

(b)

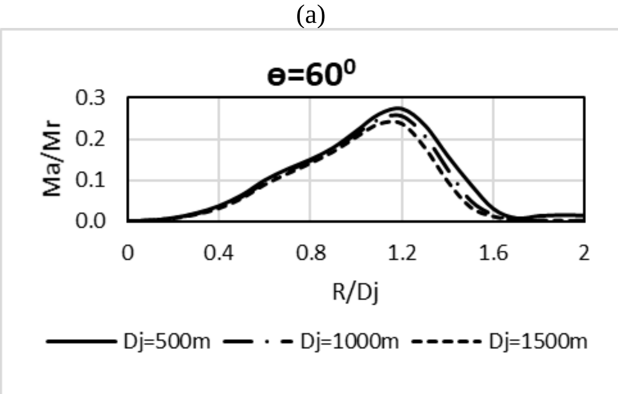

(c)

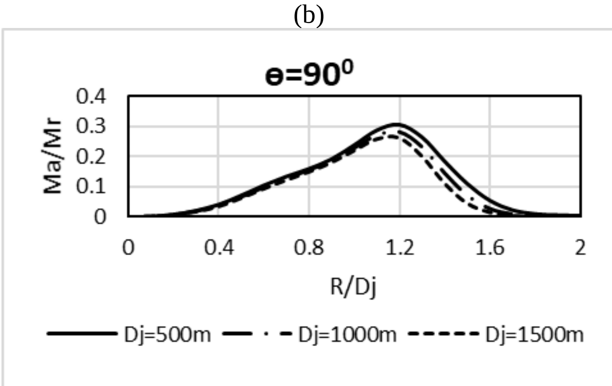

(d)

Fig. 24 (a)-(d) Variation of (M_a/M_r) with R/D_j

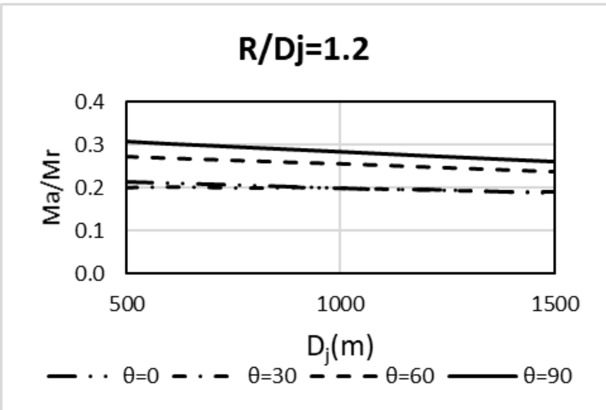

Fig. 25 Variation of (M_a/M_r) with Dj

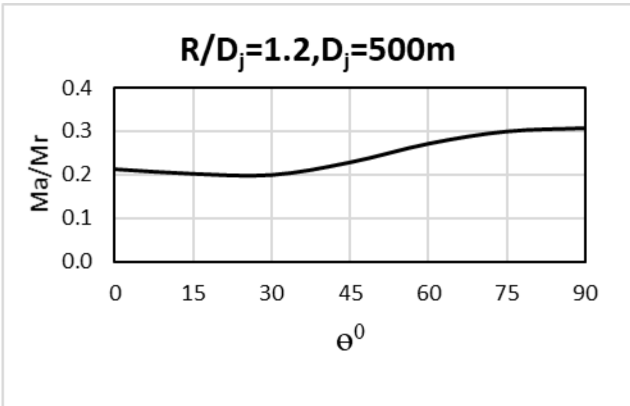

Fig. 26 Variation of (M_a/M_r) with θ

9.2 Guy1 forces

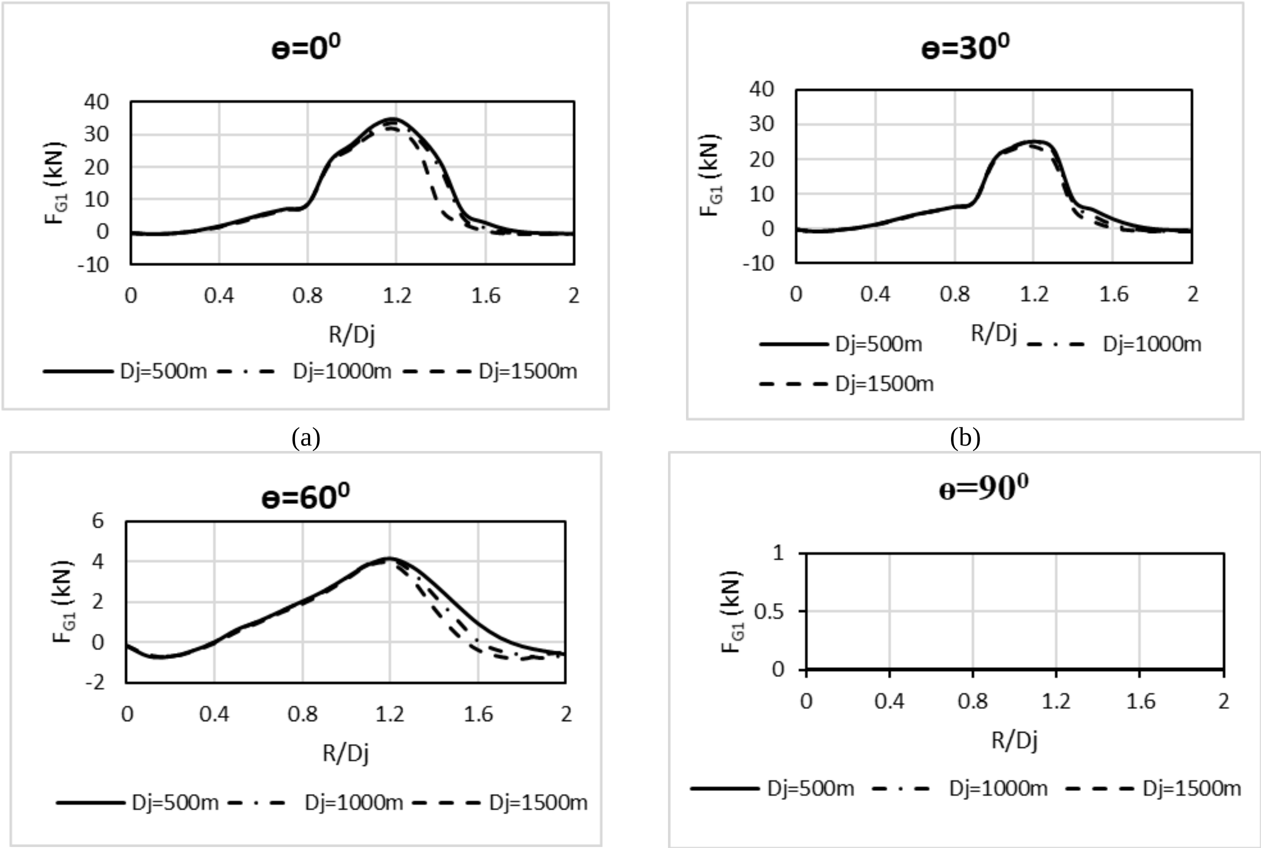

(a) (b)

(c) (d)

Fig. 27 (a)-(d) Variation of F_{G1} with R/D_j

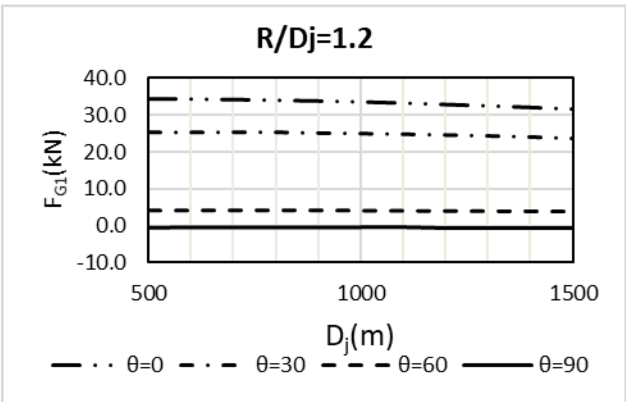

Fig. 28 Variation of F_{G1} with D_j

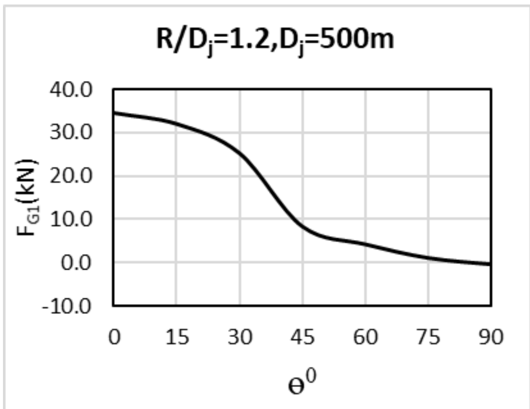

Fig. 29 Variation of F_{G1} with θ

9.3 Guy2 forces

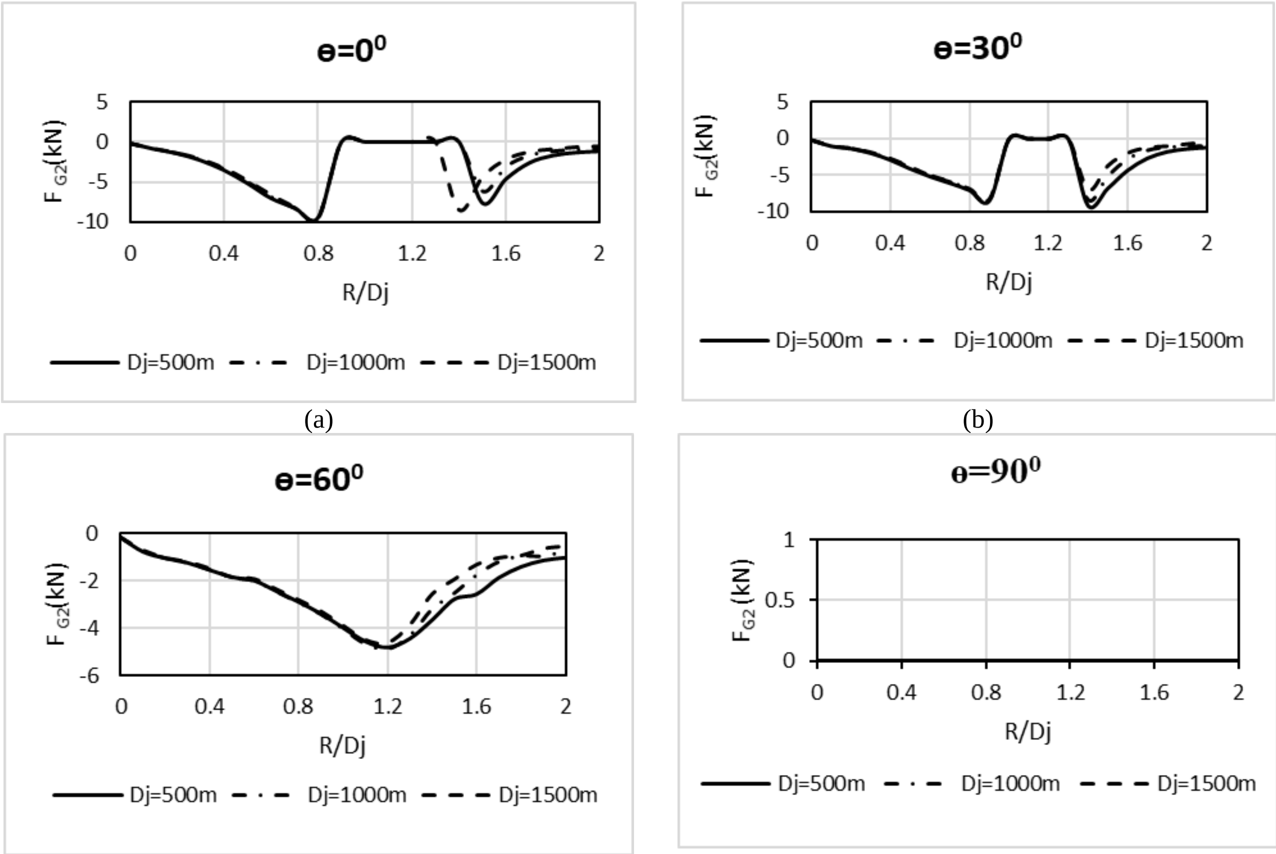

(a) (b)

(c) (d)

Fig. 30 (a)-(d) Variation of F_{G2} with R/D_j

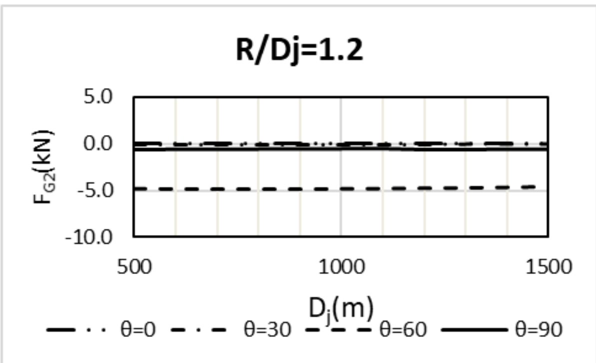

Fig. 31 Variation of F_{G2} with D_j

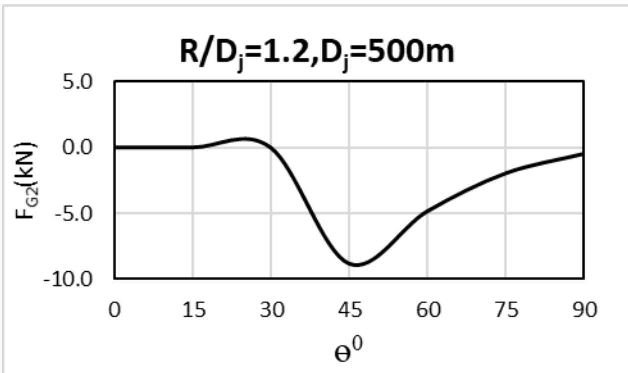

Fig. 32 Variation of F_{G2} with θ

Appendix B

Results of the guyed pole with conductor spans of 300 m

10.1 Pole bending moment

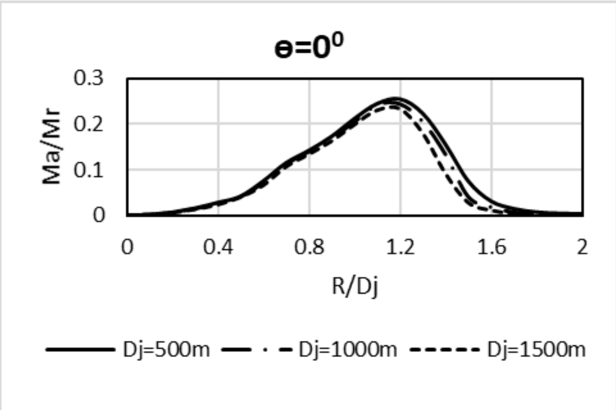

(a)

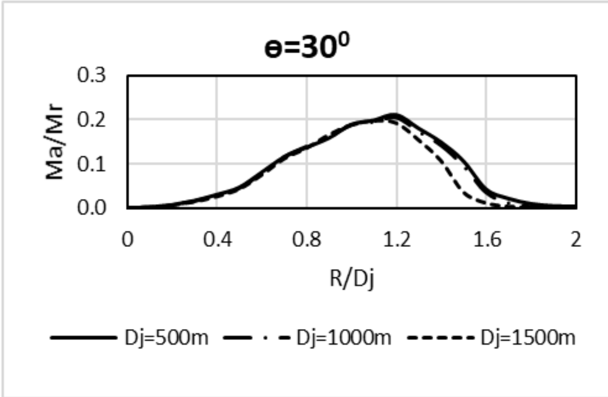

(b)

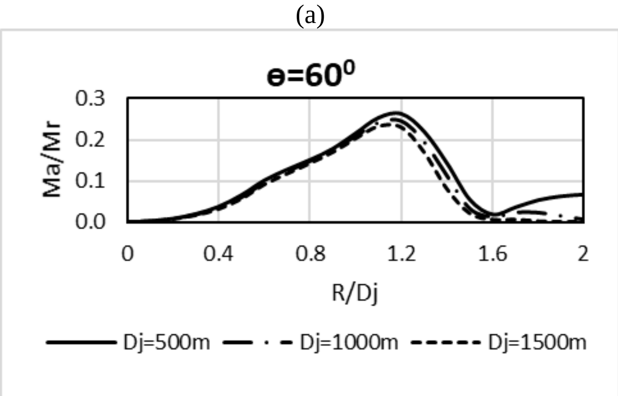

(c)

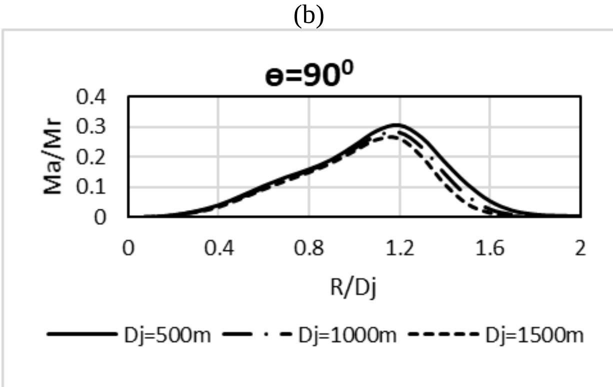

(d)

Fig. 33 (a)-(d) Variation of (M_a/M_r) with R/D

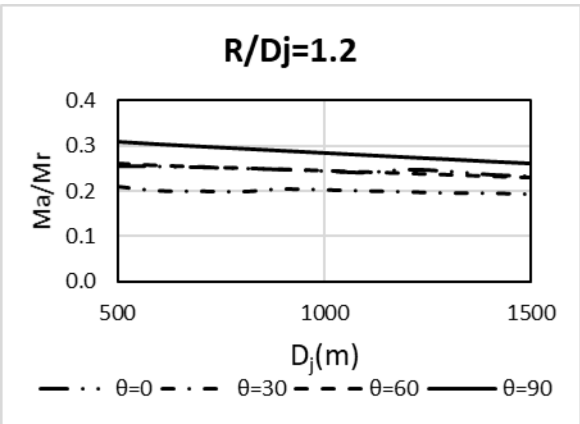

Fig. 34 Variation of (M_a/M_r) with Dj

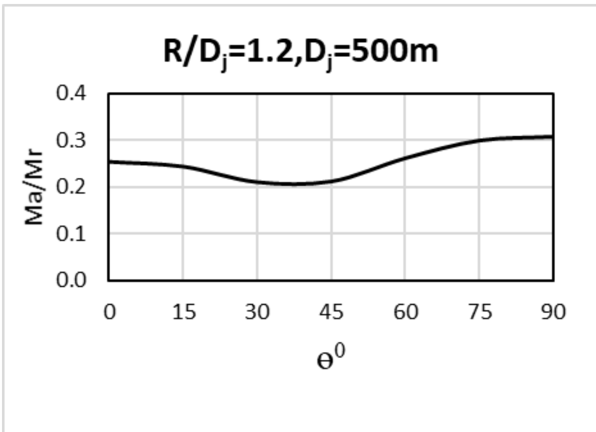

Fig. 35 Variation of (M_a/M_r) with θ

10.2 Guy1 forces

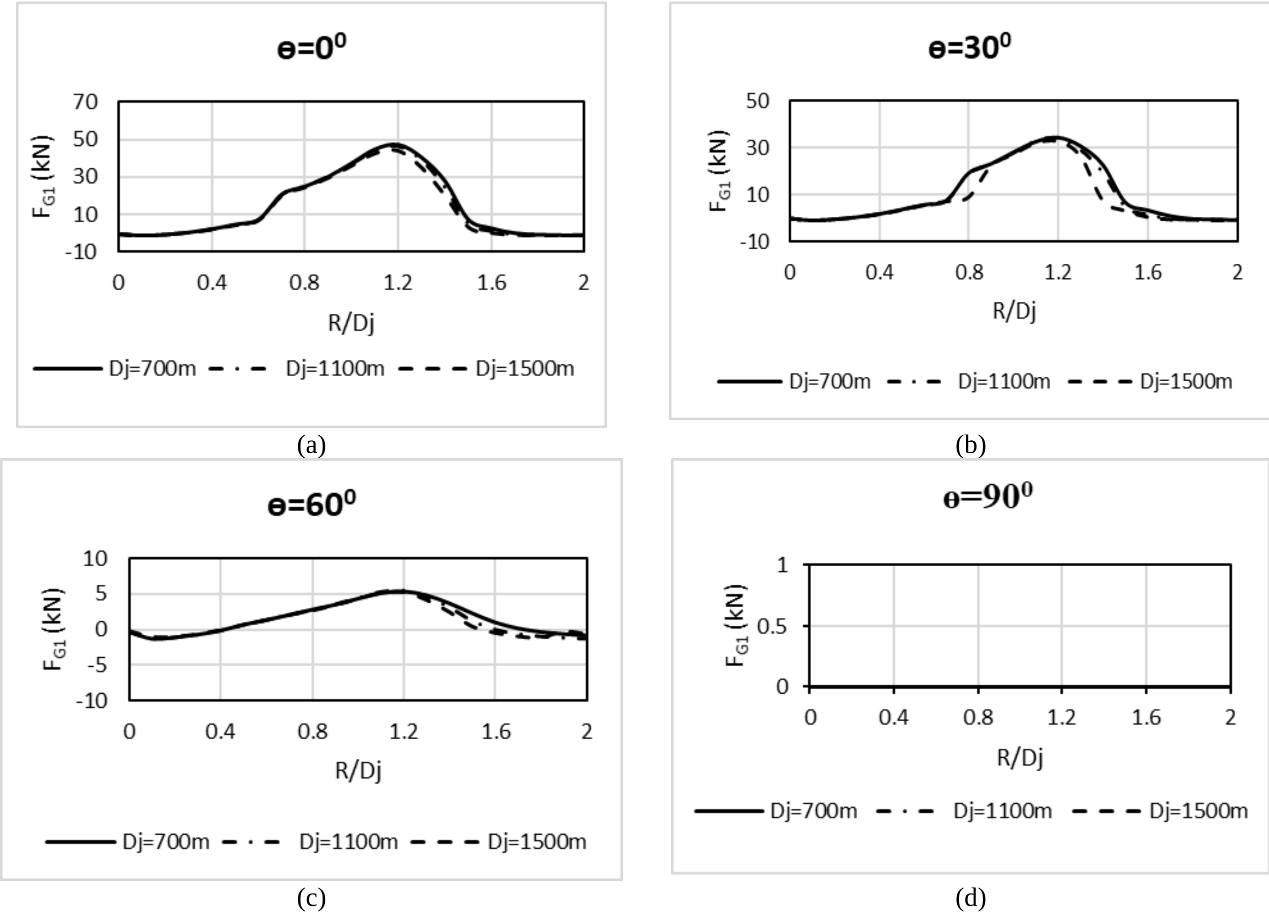

Fig. 36 (a)-(d) Variation of F_{G1} with R/D_j

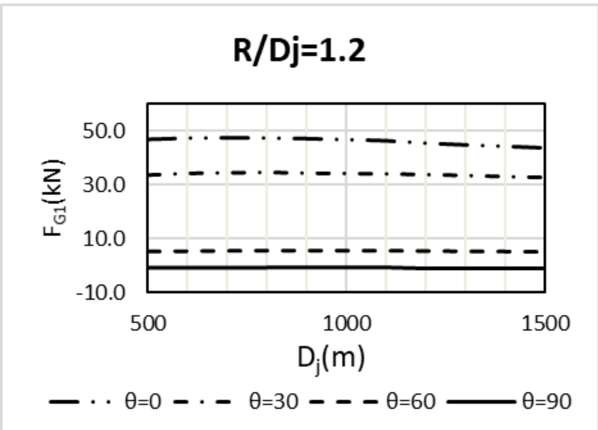

Fig. 37 Variation of F_{G1} with D_j

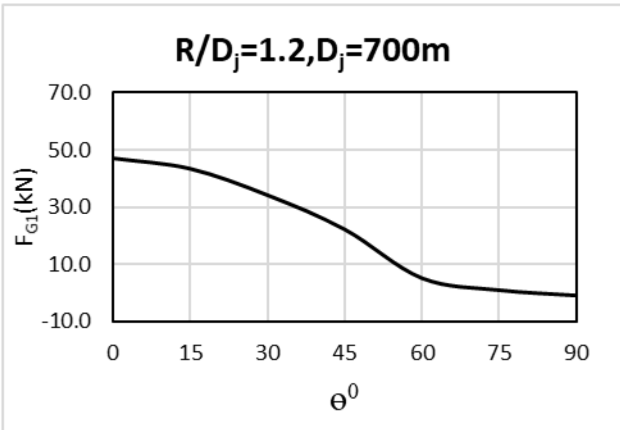

Fig. 38 Variation of F_{G1} with θ

10.3 Guy2 forces

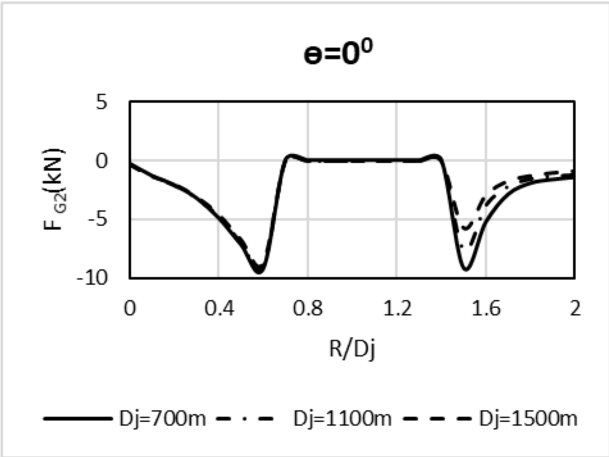

(a)

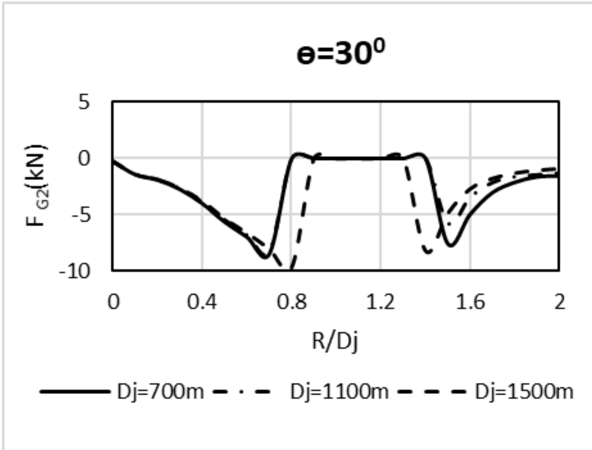

(b)

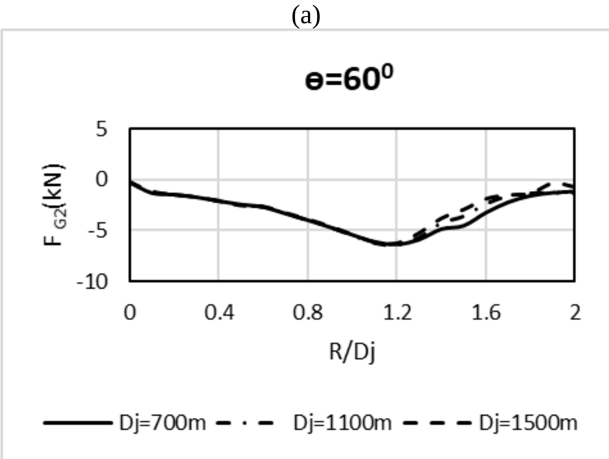

(c)

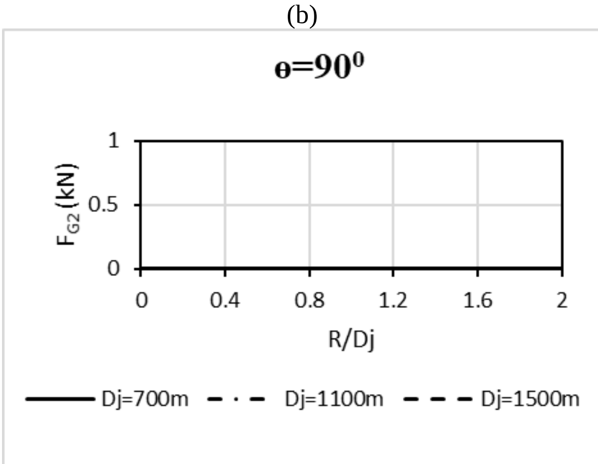

(d)

Fig. 39 (a)-(d) Variation of F_{G2} with R/D_j

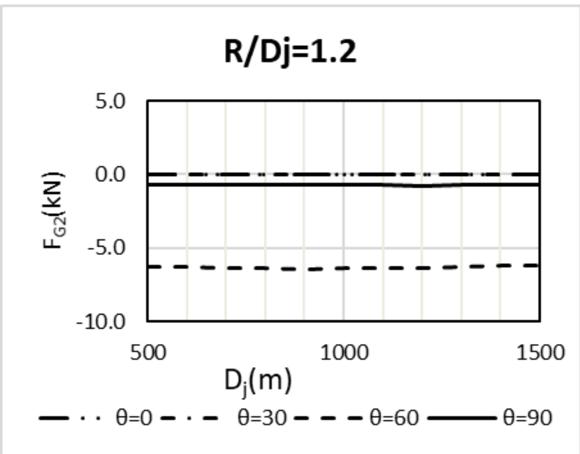

Fig. 40 Variation of F_{G2} with D_j

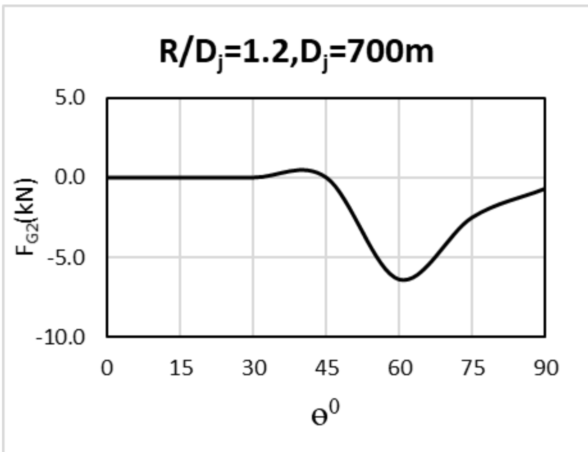

Fig. 41 Variation of F_{G2} with θ